Combined molecular beam epitaxy and diffractometer system for *in situ* x-ray studies of crystal growth

Bernd Jenichen,[a] Wolfgang Braun, Vladimir M. Kaganer, Alexander G. Shtukenberg, Lutz Däweritz, Carl-Günther Schulz, and Klaus H. Ploog
Paul-Drude-Institut für Festkörperelektronik, Hausvogteiplatz 5–7, D-10117 Berlin, Germany

Alexei Erko
BESSY GmbH, Albert-Einstein-Strasse 15, D-12489 Berlin, Germany

(Received 26 August 2002; accepted 8 October 2002)

A combination of a molecular beam epitaxy (MBE) machine and a six circle diffractometer has been constructed at a dedicated wiggler beamline at the storage ring BESSY II for *in situ* investigations of III–V compound crystal growth. The growth conditions in our system reach a high MBE standard with a noncooled base pressure of 2×10^{-10} mbar. A fast entry load lock is available for sample exchange. Large-area Be windows in the ultrahigh vacuum chamber allow us to measure reflections at entrance and exit angles up to 45°, i.e., large perpendicular momentum transfers are possible. *In situ* reflection high energy electron diffraction and x-ray fluorescence measurements can be performed simultaneously with x-ray scattering. A GaAs(001) surface prepared and examined in our system reveals terrace widths of 450 nm and $\beta(2\times4)$ reconstruction domain sizes of 210 nm. The possibility of time-resolved x-ray diffraction studies is demonstrated by observation of intensity oscillations during layer-by-layer homoepitaxial growth on the GaAs(001)$\beta(2\times4)$ surface. The resolution functions of our experiment are determined. © *2003 American Institute of Physics.* [DOI: 10.1063/1.1535237]

I. INTRODUCTION

Due to the weak x-ray–matter interaction, surface x-ray scattering can be interpreted using kinematical theory, thus providing quantitative information on the structure and morphology of the surface. The methods of surface diffraction are well established and the use of synchrotron radiation has allowed an accurate structural analysis of many types of reconstructed surfaces,[1–7] studies of the surface morphology[8–17] and defects of heteroepitaxial interfaces.[18]

A further step is the it *real-time* observation of the growing surface. Several time-resolved studies of molecular beam epitaxial (MBE) growth were performed.[19–23] The metalorganic vapor-phase epitaxy (MOVPE) of semiconductors was also studied by means of time-resolved x-ray scattering[24–29] using specially developed vertical flow MOVPE chambers.[30,31] In addition, the heteroepitaxy of GaN on Al_2O_3 by gas source MBE was investigated.[32]

Recently developed surface diffractometers allow measurements at large incidence and exit angles in order to obtain a good accuracy of the atomic coordinates perpendicular to the surface. A surface diffractometer using an in-vacuum x-ray detector was developed,[33] which can measure at exit angles up to 90°. An alternative approach is the use of large Be windows, which allow incidence and exit angles of 45° and increase the freedom of sample movement.[34–36]

The present article describes a combination of a solid-source MBE equipment for the growth of III–V based compounds and a six-circle diffractometer for the *in situ* observation of surface x-ray scattering and reflectivity during the MBE growth process. It is installed at the PHARAO beamline U125/2-KMC at the storage ring BESSY II (Berlin, Germany). We also determine the resolution of the x-ray diffraction experiment and demonstrate, as a first example of time-resolved x-ray intensity measurements, quantitative studies of the layer-by-layer growth of the $\beta(2\times4)$-reconstructed GaAs(001) surface.

II. EXPERIMENTAL SETUP

The experimental setup consists of a multiple solid-source MBE chamber inside a six-circle diffractometer shown in Fig. 1.[37] It is established at a dedicated beamline.

A. Beamline

The x-ray source is an undulator installed in a high beta section of the orbit of the storage ring BESSY II. This undulator has 32 periods, each with a length of 125 mm, and a variable magnet gap from 40 to 15.7 mm. The critical photon energy of the undulator on the axis is 2.6 keV. The average power emitted by the undulator into an angular range of 1 mrad horizontally and integrated vertically is 160 W at 100 mA beam current. The specified horizontal and vertical sizes of the x-ray source are 0.76 mm and 0.2 mm, respectively. The undulator is operated in the wiggler mode for surface diffraction experiments.

The designed energy range of the beamline is 6–12 keV. The x-ray beam is shaped by means of four independent water-cooled slits located 22 m from the source. The low-energy part of the spectrum is absorbed by a water-cooled Be foil placed behind the slits. A toroidal pre-mirror, located

[a]Electronic mail: jen@pdi-berlin.de

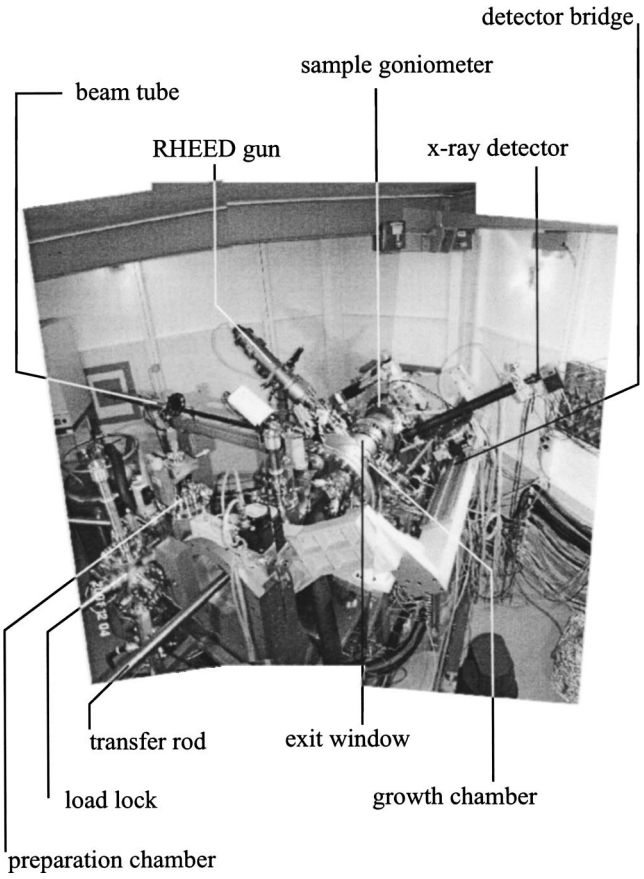

FIG. 1. MBE system with surface diffractometer. The RHEED gun, the incident beam tube, and the detector flight tube are at positions close to the sample surface plane. The transfer rod in front is perpendicular to the sample surface. The sample is rigidly connected to the sample goniometer and all the movements of this goniometer are transferred into the UHV using a rotary feedthrough connected to externally stabilized bellows.

23.4 m from the source, collimates the beam for the double crystal monochromator (DCM, 26.6 m from the source). The pre-mirror is a water-cooled Si substrate coated with a Rh reflecting layer. The long radius of the mirror is 10.4 km and the short radius 204 mm. The DCM consists of two flat Si(111) crystals at present achieving an energy resolution of $\Delta E/E \cong 7\times 10^{-4}$ as experimentally determined from the dispersion obtained by measurements of the sample rocking curve widths (see Sec. III) at 12 keV x-ray energy. The first monochromator crystal is water cooled directly from the backside. The second mirror chamber contains two mirrors that can be used alternatively. One is toroidal, with a long radius of 4.1 km and a short radius of 79.5 mm. This mirror is used for focusing the beam on the center of the diffractometer. The second is a plane mirror for parallel (minimum divergence) illumination of the sample. Both mirrors are Rh-coated Zerodur blocks. Special emphasis was put on the machining of the mirror surfaces to minimize the slope errors. The toroidal mirror was designed to produce a spot size of 0.2 mm$\times$0.5 mm (vertical$\times$horizontal) at the experiment (center of the diffractometer), which is located at a distance of 39 m from the source. The experimentally observed focus size is well within 1 mm^2. The divergence of the x-ray beam at the experiment is 0.08 mrad$\times$0.8 mrad (vertical $\times$horizontal, see also Sec. III). Beam monitors are available immediately behind each mirror. The monitor behind the second mirror can also be used to image the beam from the monochromator by moving the second mirror out of the beam.

TABLE I. Angular ranges and resolutions of the diffractometer axes in degrees. The notation follows Ref. 38.

Purpose	Axis	Range	Resolution
Incidence angle	α	0°–45°	0.02°
Sample tilt by double cradle	χ	−3°–+3°	0.001°
Rotation of double cradle	ϕ	0°–360°	0.001°
Sample rotation	ω	0°–360°	0.001°
Detector azimuthal rotation	δ	0°–130°	0.001°
Detector polar angle	γ	0°–45°	0.001°

B. Diffractometer

The horizontal axis diffractometer (horizontal sample normal) follows the example of other existing instruments for surface diffraction.[1,34–36] The angular ranges of the diffractometer are given in Table I, together with the notation of the diffractometer axes used in Ref. 38. The center of the diffractometer is placed onto the beam axis by means of two perpendicular motorized linear translations. The sphere of confusion of the diffractometer has a radius of 0.02 mm. We can perform grazing incidence diffraction[39] in the *z*-axis geometry[38,40] in an extended range along the crystal truncation rods (see Table I). The incidence angle α is varied by rotating the whole diffractometer around the vertical axis. The ϕ and χ stages are mounted on the ω stage of the sample goniometer. The surface normal is aligned along the horizontal diffractometer axis with the χ (tilt) and the ϕ circles by reflecting a laser beam from the sample surface during ω rotation of the sample. This alignment is usually fine tuned by observation of the reflected x-ray beam with a linear detector behind the exit window. The δ circle of the detector uses the same horizontal axis as the ω stage[38] and allows for in-plane (with respect to the sample surface) movement of the detector. The γ circle of the detector for out-of-plane movements is realized via a combination of rotation and translation on the detector bridge allowing for heavy detectors and ensuring a high stability of measurements with analyzer crystals.[34] The distance between the sample and the detector increases with increasing γ. Orthogonal pairs of motorized slits are mounted 40 cm (S1) and 100 cm (S2) behind the sample, at the two ends of the detector flight tube. In most cases, all vertical slits (parallel to the sample surface) are set at 2 mm, cutting an appropriate region of the crystal truncation rod (CTR), and the horizontal ones are set at 10 mm. In addition to the usual scintillation counter, energy dispersive detectors (Si drift diodes) can be used inside and outside the UHV chamber in order to observe fluorescence radiation. The diffractometer is driven by three-phase stepper motors and controlled by the TASCOM[41] software.

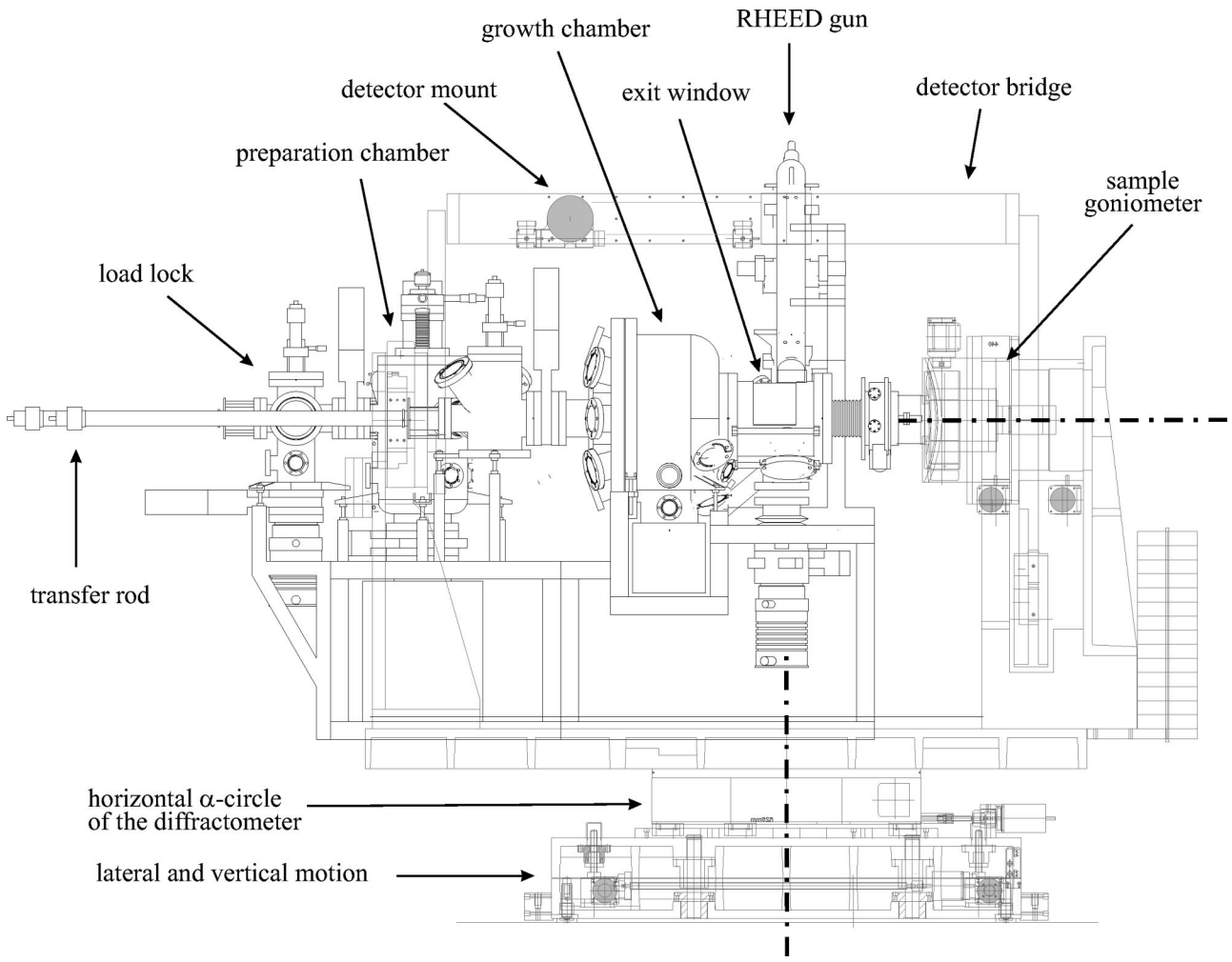

FIG. 2. Schematic drawing of the MBE system (black lines) with surface diffractometer (gray lines). The sample is positioned at the intersection of the vertical and horizontal axes of the diffractometer. The incident x-ray beam going through this intersection point is perpendicular to the plane of the drawing. The detector mount on the linear table of the detector bridge is shown here at an unusual position.

C. MBE system

The diffractometer contains a fully equipped solid-source MBE system as shown schematically in Fig. 2. The sample is fixed inside the UHV growth chamber using custom-designed Mo sample holders for quarters of 2 in. wafers of different thicknesses. The sample holder is mounted on a heating stage rigidly connected to the ϕ circle of the diffractometer. The ϕ and ω movements are transferred into UHV using a two-stage differentially pumped rotary feedthrough further encapsulated in a noble gas atmosphere in order to prevent contamination by air in case of a leak. The double cradle χ movements are enabled using externally stabilized welded bellows.

The growth chamber has two large-area Be windows protected from coating by inside 0.1 mm Be foils. The total thickness of each window is 0.6 mm. The size of the windows allows for entrance and exit angles up to 45°, i.e., large angular momentum transfers (similar to Refs. 34–36). We preferred to place the movable detectors outside the UHV chamber, in order to have the free choice of the type and resolution of the detector at any time. The growth chamber is pumped by ion, turbo-molecular and Ti sublimation pumps maintaining a base pressure of 2×10^{-10} mbar without liquid nitrogen cooling. In addition, it features liquid nitrogen cooled shrouds around the effusion cells and around the substrate. In this way, standard MBE conditions are obtained. The MBE system is equipped with seven simultaneously operating effusion cells. At present six of them are already filled with Ga, As, Al, In, Sb, and Mn. This allows us to grow a large variety of semiconducting and magnetic III–V compounds. A fast entry load lock is available for easy sample exchange. An intermediate preparation chamber allows for heat treatment of the samples prior to the growth experiment. From this chamber the cleaned samples are then transferred into the growth chamber, where as a first step the oxide desorption is performed.

For our first study, only Ga and As were used. The As was evaporated from a noncracking valved source, Ga from a two-zone hot-lip cell. The Ga cell is mounted in a position symmetrical to the substrate. Since Ga is the rate-limiting element during growth, this minimizes growth oscillation damping effects due to growth rate variations across the wafer.[42]

MBE growth is controlled with a high-precision reflection high-energy electron diffraction (RHEED) setup, mounted at an angle of 43° to the x-ray beam. Figure 3

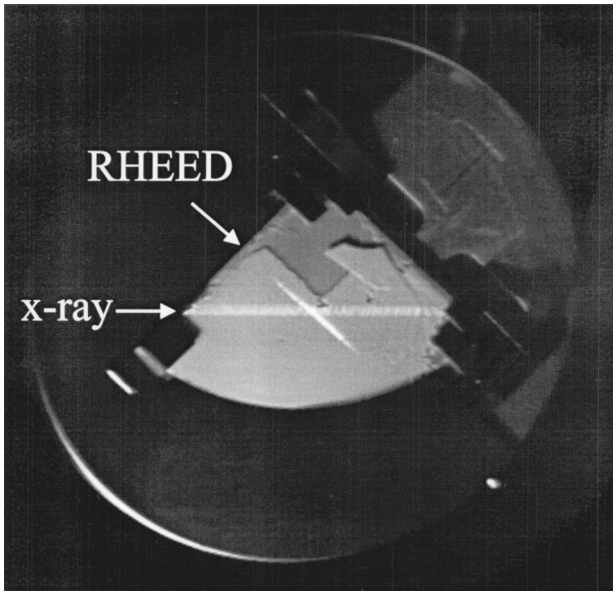

FIG. 3. Photograph of a fluorescent screen at the sample position with images of the x-ray beam and the electron beam at grazing incidence, differing by an azimuthal angle of 43°.

shows a photograph of a fluorescent screen at the sample position, revealing fluorescent images of the x-ray and electron beams at grazing incidence, differing by the azimuthal angle of 43 °. The RHEED gun can be operated during synchrotron x-ray illumination of the sample, allowing the simultaneous acquisition of x-ray diffraction and RHEED data. *In situ* x-ray fluorescence measurements are possible with a retractable energy-dispersive detector, which is installed behind a 50-μm-thick Be foil. A quadrupole mass spectrometer is also available for the detailed analysis of the residual gas in the UHV system. The substrate temperature is controlled by a thermocouple behind the sample.

The MBE together with the diffractometer are placed in a radiation safety hutch with interlock system.

D. Sample preparation and reciprocal lattice definition

GaAs(001) epi-ready substrates were used. The substrates were first degassed at 100 °C in the load-lock chamber, then baked for 1 h at 500 °C in the intermediate preparation chamber before being introduced into the growth chamber. The oxide was desorbed inside the growth chamber under RHEED control while heating the sample at a rate of 10 °C/min. As is common in MBE, the oxide desorption temperature is taken as 580 °C, serving as a temperature reference for the subsequent measurements.[43] With new sample holders used, temperature drifts of up to 20 °C may occur.

The As_4/Ga (V/III) flux ratio was determined from As-limited RHEED oscillations.[44] From run to run, the As_4 flux was monitored and adjusted by means of a Bayard–Alpert vacuum gauge close to the sample position. The growth conditions were optimized first by scanning the substrate temperature through the stability range of the $\beta(2\times4)$ surface reconstruction and then fine tuning the growth temperature around the center of this temperature interval by minimizing the damping of the RHEED intensity oscillations.

The (2×4) surface unit cell is rotated by 45° with respect to the cubic zinc blende unit cell of the bulk GaAs. Direction vectors, crystal planes and diffraction indices applied in this work refer to the bulk unit cell. Following the usual convention, the $[110]$ axis runs along the long edge of the (2×4) surface unit cell, the $[\bar{1}10]$ axis is parallel to the short edge.

III. RESOLUTION

A. Resolution at grazing incidence and exit angles

We checked the resolution of the setup by x-ray diffraction experiments performed with a detector, the entrance window of which is limited by slits, as described in Sec. II B, with a typical acceptance angle of 0.1°. The resolution strongly depends on the momentum transfer in the surface normal direction. When the normal component of the momentum transfer is small, i.e., both the incident and the scattered beams make small angles to the sample surface, the detector acceptance angle is irrelevant and the resolution is determined by the collimation of the incident beam and its monochromaticity. This case is considered in the present section. We describe this in some detail with the aim to use it as a reference for the analysis of the resolution for larger normal momentum transfers in Sec. III B. Section III B also establishes the limits of applicability of the results obtained here.

The reciprocal-space geometry of a surface scattering experiment is shown in Fig. 4(a) for the case when both the incident $\mathbf{k}_i$ and the diffracted $\mathbf{k}_f$ waves are in the surface plane. The angle δ between $\mathbf{k}_i$ and $\mathbf{k}_f=\mathbf{k}_i+\mathbf{q}$ (where we follow the notation of angles in Table I and $\mathbf{q}$ is the scattering vector) is equal to 2θ, where θ is the Bragg angle. For a given crystal orientation, the angular range of the incident waves which are scattered by the sample is limited by the dynamical diffraction laws. Other orientations of the incident waves do not contribute to the scattering since, for these waves, the vector $\mathbf{k}_i+\mathbf{q}$ does not fall on the Ewald sphere and elastic scattering is not possible. When the sample is rotated about its normal in an ω scan and the direction of the scattering vector $\mathbf{q}$ changes, the triangle formed by the vectors $\mathbf{k}_i$, $\mathbf{q}$, and $\mathbf{k}_f$ [broken lines in Fig. 4(a)] is rotated as a whole, the vectors remain on the Ewald sphere, and the scattering takes place in the angular range $\Delta\omega=\Delta\theta$. $\Delta\theta$ is the angular divergence of the incident beam in the surface plane. This range is small compared to the angular width of the detector $\Delta\delta$, so that the detector does not limit the resolution. Similar considerations of the length variation of the wave vectors $\mathbf{k}_i$ and $\mathbf{k}_f$ due to the dispersion $\Delta\lambda/\lambda$ of the incident beam give $\Delta\omega=(\Delta\lambda/\lambda)\tan\theta$, and we finally obtain the in-plane resolution

$$\Delta\omega=\Delta\theta+\frac{\Delta\lambda}{\lambda}\tan\theta. \tag{1}$$

Figure 4(b) presents the full widths at half-maxima (FWHMs) $\Delta\omega$ of several in-plane bulk reflections. The FWHMs were determined from Gaussian fits to the measured peaks. From a linear fit to Eq. (1) we obtain the wavelength range arriving at the sample $\Delta\lambda/\lambda=7\times10^{-4}$ and the

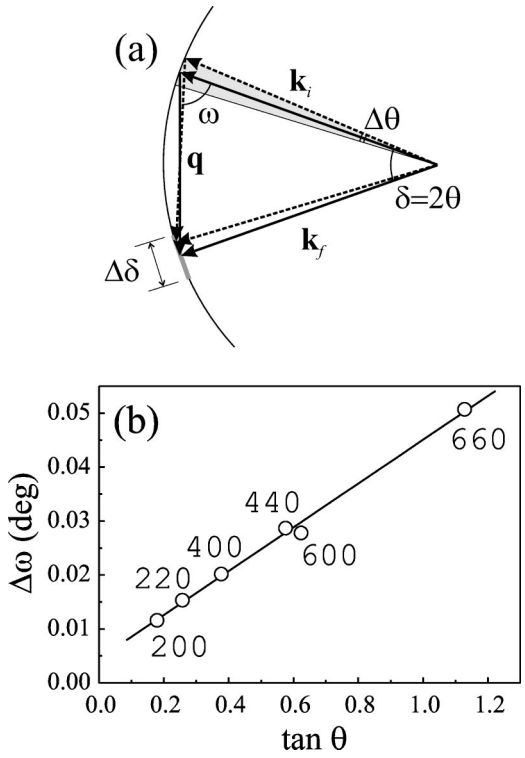

FIG. 4. (a) Reciprocal space geometry of a surface scattering experiment with grazing incidence and exit beams: $\delta=2\theta$ is the angle between the incident and the diffracted beams, θ is the Bragg angle, $\Delta\theta$ is the divergence of the incident beam, $\Delta\delta$ is the angular acceptance of the detector in the plane of the sample surface. (b) The experimentally determined full width at half maximum (FWHM) of ω scans for different in-plane bulk reflections from a GaAs(001) crystal plotted over tan θ. The x-ray wavelength is 0.1 nm.

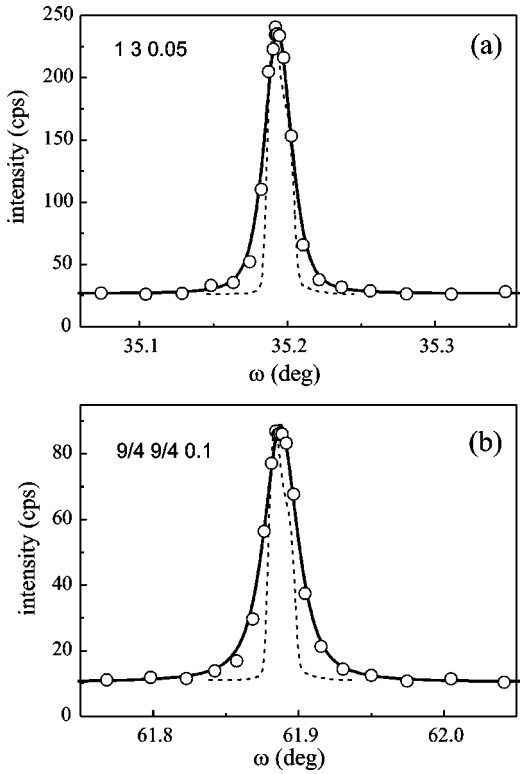

FIG. 5. The ω scans of an integer order surface diffraction peak 1 3 0.05 (a) and a fractional order peak 9/4 9/4 0.1 (b) of the GaAs(001)$\beta(2\times4)$ surface (circles). Solid lines are fits to the Voigt function. The broken lines are the ω scan of the in-plane bulk reflection 220 used as the resolution function.

angular divergence of the incident beam in the surface plane $\Delta\theta=0.08$ mrad. Similar measurements in the direction perpendicular to the surface plane give $\Delta\alpha=0.8$ mrad.

Figure 5 illustrates the quality of the GaAs(001) surface prepared in our system and the available in-plane resolution by ω scans obtained in the integer-order reflection 1 3 0.05 and in the fractional order reflection 9/4 9/4 0.1. The sample preparation followed the procedures described in Sec. II D. The measured peak profiles are fitted to the Voigt function (the convolution of a Lorentzian intrinsic peak profile with a Gaussian resolution function). The FWHM of the Gaussian resolution function is taken from the linear interpolation between the FWHMs of the bulk reflections, Fig. 4(b). The peak profile of the 220 reflection, which has the Bragg angle fairly close to those of the measured in-plane reflections, is shown in Figs. 5(a) and 5(b) by broken lines. We make the Voigt function fit with fixed width of the Gaussian component and variable width of the Lorentzian component, so that the number of fit parameters is the same as in a Gaussian or Lorentzian fit. We find that the Voigt function fit gives smaller χ^2 values than the two latter functions. Hence, the intrinsic peak profiles of both integer- and fractional-order peaks are Lorentzians, which indicates exponential correlation functions.

The correlation length $\ell=2/(q\Delta\omega)=450$ nm obtained in the integer-order reflection 1 3 0.05 is the mean terrace width.[45,46] The correlation length of 210 nm obtained in the fractional order reflection 9/4 9/4 0.1 characterizes the reconstruction domain sizes. These values are larger by a factor of 5 than the terrace and reconstruction domain sizes obtained in a previous *ex situ* room-temperature x-ray diffraction study of the quenched GaAs(001) surface with the same reconstruction as in our experiment.[4] The large terrace and domain sizes are reached in our system thanks to the optimized MBE growth conditions and the possibility of *in situ* x-ray scattering measurements at growth temperature.

B. Resolution at grazing incidence and nongrazing exit angles

The analysis of the previous section cannot be applied to large momentum transfer in the surface normal direction, Fig. 6(a). Then, the angular width of the detector becomes the resolution-limiting factor.[38,47] Let us denote by $\Delta\gamma$ and $\Delta\delta$ the angular widths of the detector in the directions perpendicular and parallel to the sample surface, respectively. The polar angle γ and the azimuth δ with respect to the incident beam define the orientation of the diffracted wave vector $\mathbf{k}_f$, Fig. 6(a) (we follow the notation of the diffractometer circles, see Table I). The segment of the Ewald sphere limited by the angular ranges $\Delta\gamma$ and $\Delta\delta$ around the direction of the scattered wave defines, projected to the surface plane, the ranges of the wave vectors along the scattering vector, $\Delta q_\parallel$, and normal to it, $\Delta q_\perp$, equal to

$$\Delta q_\parallel = k\sin\gamma\Delta\gamma, \quad \Delta q_\perp = k\cos\gamma\Delta\delta, \tag{2}$$

where $k=2\pi/\lambda$ is the wave vector.

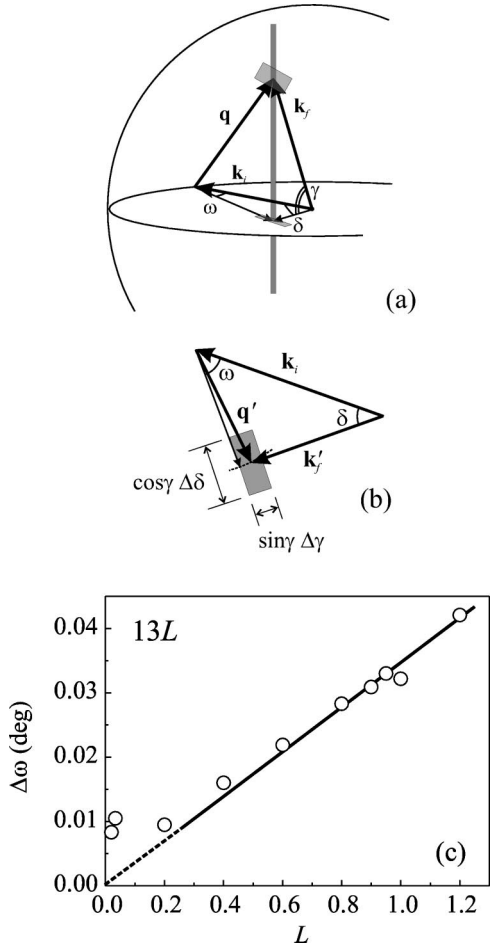

FIG. 6. (a) Reciprocal space geometry of a grazing incidence surface scattering experiment and (b) the projection of the wave vectors on the sample surface plane in the case of grazing incidence and nongrazing exit. The shadowed rectangle corresponds to the angular width of the detector and its projection on the surface plane. (c) Full widths at half-maximum (FWHM) of ω scans along the crystal truncation rod 13L of the GaAs(001) $\beta(2\times4)$ surface.

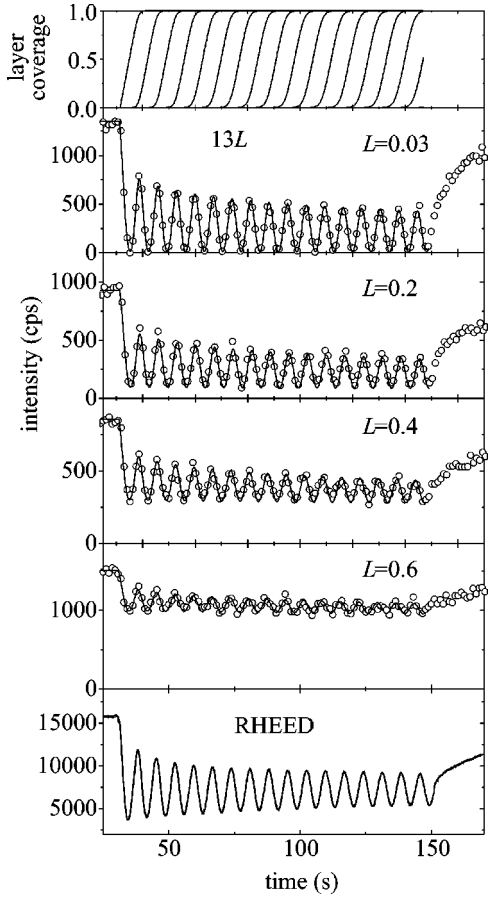

FIG. 7. X-ray intensity oscillations measured during MBE growth of GaAs(001) at different points along the crystal truncation rod 13L (open circles). The fit (solid curves) is obtained simultaneously for all curves with the layer coverage shown in the top panel of the figure. In the bottom panel the oscillating RHEED intensity of the specular beam measured simultaneously is given in arbitrary units. For these measurements the reflected RHEED beam forms an angle of 76° with the diffracted x-ray beam. The substrate temperature was 570 °C.

When the sample is rotated about its normal in the ω scan, the crystal truncation rod (CTR) crosses a segment of the Ewald sphere which corresponds to the angular width of the detector, Fig. 6(a). On the sample surface plane, Fig. 6(b), the projection **q** of the scattering vector **q** rotates and crosses the resolution range (2). The angular width of the ω scan given by the detector width is

$$\Delta\omega = \min\left(\frac{\sin\gamma}{\sin\delta}\Delta\gamma,\quad \frac{\cos\gamma}{|\cos\gamma-\cos\delta|}\Delta\delta\right), \tag{3}$$

where the two terms on the right-hand side of Eq. (3) correspond to crossing one of the two orthogonal sides of the shadowed rectangle in Fig. 6(b).

In the present study, the polar angle γ was relatively small, $\gamma<20°$, and the first term in Eq. (3) is then smaller than the second one. Taking into account that $\sin\gamma=\lambda L/a$, where a is the lattice period and L is the continuous Miller index along a CTR, we find that the angular width of the ω scan is proportional to L, $\Delta\omega=\lambda L\Delta\gamma/(a\sin\delta)$, if the weak dependence of the azimuth δ on L is neglected. This linear dependence is clearly seen in the measured dependence of the FWHM of the ω scans along the CTR 13L, Fig. 6(c). From the slope of the line, we obtain the angular width of the detector $\Delta\gamma=0.1°$, in good agreement with the value obtained from the nominal width of the vertical detector slits and the distance between them (see Sec. II B). One can see from Fig. 6(c) that the linear dependence on L, and hence the detector width as a resolution-limiting factor, is important for $L>0.2$. It follows from Fig. 6(c) that at $L=0.6$, the resolution decreases by a factor of 2 compared with the in-plane resolution, by a factor of 4 at $L=1.2$, etc.

IV. X-RAY INTENSITY OSCILLATIONS DURING LAYER-BY-LAYER GROWTH

We performed time-resolved x-ray intensity measurements at different points L along the CTRs 13L, Fig. 7. The background intensity is obtained from sufficiently wide ω scans of the sample prior to growth and subtracted from the measured intensity. The period of the intensity oscillations $\tau=7$ s is the time required to complete one Ga–NAs bilayer of the GaAs(001) crystal. The solid lines in the intensity plots of Fig. 7 are calculated with the layer coverages presented in the top panel. The mathematical model for the coverages is described elsewhere.[48] The fit of the intensity

curves is obtained simultaneously, i.e., with the same time dependence of layer coverages, for all values of L. Due to the bulk atomic structure of GaAs, the destructive interference between subsequent atomic layers (antiphase condition) is realized at $L=0$. At small L, the intensity decreases to zero at the minimum of the first oscillation, indicating that only one layer is partially covered at that moment. However, the following maxima do not reach the initial intensity, which means that the next layer starts to grow somewhat before the previous one is completed. The growth is close to perfection, with the next layer having less than 10% coverage when the previous one is filled to about 90%. At higher values of L, the minima are no longer near zero. The surface sensitivity is decreasing with rising L, as we move away from the bulk forbidden reflection 130 towards the bulk reflection 131. Typical RHEED intensity oscillations of the specular beam obtained simultaneously with the x-ray measurements are shown for comparison in the bottom panel of Fig. 7. By measuring x-ray intensity oscillations during growth at different points L along the crystal truncation rod $13L$ of the $\beta(2\times4)$-reconstructed GaAs(001) surface, submonolayer sensitivity of our surface diffraction experiment is proven. We also demonstrate, that a detailed quantitative analysis of growth kinetics during MBE is possible.

ACKNOWLEDGMENTS

The authors would like to thank S. Brennan, R. Feidenhans'l, S. Ferrer, A. Fischer, M. Höricke, R. Köhler, W. Moritz, I. K. Robinson, and M. Schmidbauer for their advice and support during the design phase of the beamline and the experimental setup.

[1] R. Feidenhans'l, Surf. Sci. Rep. **10**, 105 (1989).
[2] I. K. Robinson and D. J. Tweet, Rep. Prog. Phys. **55**, 599 (1992).
[3] I. K. Robinson, Phys. Rev. B **33**, 3830 (1986).
[4] Y. Garreau, M. Sauvage-Simkin, N. Jedrecy, R. Pinchaux, and M. Veron, Phys. Rev. B **54**, 17638 (1996).
[5] C. Kumpf, D. Smilgies, E. Landemark, M. Nielsen, R. Feidenhaus, O. Bunk, J. H. Zeysing, Y. Su, R. L. Johnson, L. Cao, J. Zegenhagen, B. O. Fimland, L. D. Marks, and D. Ellis, Phys. Rev. B **64**, 075307 (2001).
[6] A. Munkholm, G. B. Stephenson, J. A. Eastman, C. Thompson, P. Fini, J. S. Speck, O. Auciello, P. H. Fuoss, and S. P. DenBaars, Phys. Rev. Lett. **83**, 741 (1999).
[7] A. Hirnet, K. Schroeder, S. Blgel, X. Torrelles, M. Albrecht, B. Jenichen, M. Gierer, and W. Moritz, Phys. Rev. Lett. **88**, 226102 (2002).
[8] M. Murty, T. Curcic, A. Judy, B. Cooper, A. R. Woll, J. D. Brock, S. Kycia, and R. Headrick, Phys. Rev. Lett. **80**, 4713 (1998).
[9] M. V. R. Murty, T. Curcic, A. Judy, B. H. Cooper, A. R. Woll, J. D. Brock, S. Kucia, and R. L. Headrick, Phys. Rev. B **60**, 16956 (1999).
[10] G. Renaud, P. H. Fuoss, J. Bevk, and B. S. Freer, Phys. Rev. B **45**, 9192 (1992).
[11] D. Y. Noh, K. I. Blum, M. J. Ramstad, and R. J. Birgeneau, Phys. Rev. B **48**, 1612 (1993).
[12] F. J. Lamelas, P. H. Fuoss, D. W. Kisker, G. B. Stephenson, P. Imperatori, and S. Brennan, Phys. Rev. B **49**, 1957 (1994).
[13] M. Yoon, S. G. J. Mochrie, M. W. Tate, S. M. Gruner, and E. F. Eikenberry, Phys. Rev. B **80**, 337 (1998).
[14] M. Yoon, S. G. J. Mochrie, D. M. Zehner, G. M. Watson, and D. Gibbs, Phys. Rev. B **49**, 16702 (1994).
[15] S. Pflanz, H. L. Meyerheim, W. Moritz, I. K. Robinson, H. Hoernis, and E. H. Conrad, Phys. Rev. B **52**, 2914 (1995).
[16] S. Song, M. Yoon, S. G. J. Mochrie, G. B. Stephenson, and S. T. Milner, Surf. Sci. **372**, 37 (1997).
[17] Y. Garreau, V. Repain, J. Berroir, S. Rousset, V. Etgens, and J. Lecoeur, Physica B **283**, 223 (2000).
[18] G. Renaud, P. Guénard, and A. Barbier, Phys. Rev. B **58**, 7310 (1998).
[19] E. Vlieg, A. W. D. van der Gon, J. F. van der Veen, J. E. Macdonald, and C. Norris, Phys. Rev. Lett. **61**, 2241 (1988).
[20] H. A. van der Vegt, H. M. van Pinxteren, M. Lohmeier, E. Vlieg, and J. M. C. Thornton, Phys. Rev. Lett. **68**, 3335 (1992).
[21] H. A. van der Vegt, J. Alvarez, X. Torrelles, S. Ferrer, and E. Vlieg, Phys. Rev. B **52**, 17443 (1995).
[22] J. Alvarez, E. Lundgren, X. Torrelles, and S. Ferrer, Phys. Rev. B **57**, 6325 (1998).
[23] J. Alkvarez, E. Lundgren, X. Torrelles, and S. Ferrer, Surf. Sci. **464**, 165 (2000).
[24] F. J. Lamelas, P. H. Fuoss, P. Imperatori, D. W. Kisker, G. B. Stephenson, and S. Brennan, Appl. Phys. Lett. **60**, 2610 (1992).
[25] D. W. Kisker, G. B. Stephenson, P. H. Fuoss, F. J. Lamelas, P. Imperatori, and S. Brennan, J. Cryst. Growth **124**, 1 (1992).
[26] D. Kisker, G. B. Stephenson, P. Fuoss, and S. Brennan, J. Cryst. Growth **146**, 104 (1995).
[27] P. H. Fuoss, D. W. Kisker, F. J. Lamelas, G. B. Stephenson, P. Imperatori, and S. Brennan, Phys. Rev. Lett. **69**, 2791 (1992).
[28] D. W. Kisker, G. B. Stephenson, J. Tersoff, P. H. Fuoss, and S. Brennan, J. Cryst. Growth **163**, 54 (1996).
[29] A. Munkholm, C. Thompson, G. B. Stephenson, J. A. Eastman, O. Auciello, P. Fini, J. Speck, and S. P. DenBaars, Physica B **283**, 217 (2000).
[30] S. Brennan, P. H. Fuoss, J. L. Kahn, and D. W. Kisker, Nucl. Instrum. Methods Phys. Res. A **291**, 86 (1990).
[31] G. B. Stephenson, J. A. Eastman, O. Auciello, A. Munkolm, C. Tompson, P. H. Fuoss, P. Fini, S. P. DenBaars, and J. S. Speck, MRS Bull. **24**, 21 (1999).
[32] R. L. Headrick, S. Kycia, A. R. Woll, J. D. Brock, and M. V. Ramana, Phys. Rev. B **58**, 4818 (1998).
[33] M. Ablrecht, H. Antesberger, W. Mortiz, H. Plöckl, M. Sieber, and D. Wolf, Rev. Sci. Instrum. **70**, 3239 (1999).
[34] S. Ferrer and F. Comin, Rev. Sci. Instrum. **66**, 1674 (1995).
[35] C. L. Nicklin, J. S. G. Taylor, N. Jones, P. Steadman, and C. Norris, J. Synchrotron Radiat. **5**, 890 (1998).
[36] R. Baudoing-Savois, M. De Santis, M. C. Saint-Lager, P. Dolle, O. Geaymond, P. Taunier, P. Jeantet, J. Roux, G. Renaud, A. Barbier, O. Robach, O. Ulrich, A. Mougin, and G. Bérard, Nucl. Instrum. Methods Phys. Res. B **149**, 213 (1999).
[37] The beamline was manufactured by Oxford Danfysik, UK, using mirrors made by SESO, France. The MBE unit was made by CreaTec, Germany, incorporating a custom-built diffractometer manufactured by Huber, Germany.
[38] E. Vlieg, J. Appl. Crystallogr. **30**, 532 (1997).
[39] W. C. Marra, P. Eisenberger, and A. J. Cho, J. Appl. Phys. **50**, 6927 (1979).
[40] J. Bloch, J. Appl. Crystallogr. **18**, 33 (1985).
[41] J. Bundgaard, K. Enevoldsen, and P. Skaarup, Triple Axis Spectrometer Commands (TASCOM), Risoe National Laboratory, Roskilde, Denmark, 1996.
[42] W. Braun, in *Applied RHEED*, of *Springer Tracts in Modern Physics*, Vol. 154 (Springer, Berlin, 1999), Chap. 3.1.
[43] A. J. Springthorpe, S. J. Ingrey, B. Emmerstorfer, P. Mandeville, and W. T. Moore, J. Vac. Sci. Technol. B **5**, 739 (1987).
[44] B. F. Lewis, R. Fernandez, A. Madhukar, and F. J. Gruthaner, J. Vac. Sci. Technol. B **4**, 560 (1986).
[45] S. C. Lent and P. I. Cohen, Surf. Sci. **139**, 121 (1984).
[46] P. R. Pukite, C. S. Lent, and P. I. Cohen, Surf. Sci. **161**, 39 (1985).
[47] D. Sentenac, A. N. Shalaginov, A. Fera, and W. H. de Jeu, J. Appl. Crystallogr. **33**, 130 (2000).
[48] W. Braun, B. Jenichen, V. M. Kaganer, A. G. Shtukenberg, L. Däweritz, and K. H. Ploog, Surf. Sci. (in press).